J Mater Sci (2019) 54:414–426

Composites

Poly(ε-caprolactone)/cellulose nanocrystal nanocomposite mechanical reinforcement and morphology: the role of nanocrystal pre-dispersion

Luiz G. L. Germiniani[1], Laura C. E. da Silva[1], Tomás S. Plivelic[2], and Maria C. Gonçalves[1,*]

[1] Institute of Chemistry, University of Campinas (UNICAMP), P. O. Box 6154, Campinas 13083-970, Brazil
[2] MAX IV Laboratory, Lund University, P.O. Box 118, 221 00 Lund, Sweden

Received: 17 May 2018
Accepted: 22 August 2018
Published online: 31 August 2018

ABSTRACT

Cellulose nanocrystal (CNC) incorporation in polymeric matrices is an environmentally friendly approach to mechanical reinforcement. In general, significant mechanical reinforcement can only be achieved by means of good CNC dispersion at random orientation. These primary characteristics are even more relevant for the preparation of nanocomposites based on hydrophobic matrices, such as poly(ε-caprolactone) (PCL). A straightforward approach to improve CNC dispersion in hydrophobic matrices is their surface modification. However, this extra step is usually complex and often impairs particle–particle interactions, which are also key to mechanical reinforcement. In this work, poly(ε-caprolactone)/neat cellulose nanocrystal nanocomposites were prepared by a specific procedure that combined solvent exchange and solvent casting methodologies, avoiding the use of any additives or chemical modification. These nanocomposites were investigated in terms of the CNC percolation network formation and its effect on the overall mechanical properties. The results showed that significant mechanical reinforcement was obtained, reaching a 155% Young's modulus increase at 25 wt% CNC content. TEM showed a percolated network in the PCL/CNC25 nanocomposite. In terms of morphology and nanostructure, increasing CNC concentration also promoted a reduction in PCL spherulite size and lamellar thickness. These results pointed out to CNC preferential localization in the interfibrillar region. In conclusion, the solvent exchange methodology presented herein led to mechanically reinforced PCL/CNC nanocomposites with small crystalline domains intertwined with a percolated CNC network.

Address correspondence to E-mail: maria@iqm.unicamp.br

https://doi.org/10.1007/s10853-018-2860-9

Introduction

Cellulosic nanoparticles, such as the cellulose nanocrystals (CNCs), have well-known potential as an alternative reinforcement agent for polymers, due to their abundance, low density, biodegradability and excellent mechanical properties [1, 2]. Similar to other nanoparticles, the main drawback for CNC nanocomposite preparation is to optimize dispersion, in order to reach an appropriate balance between particle–matrix and particle–particle interactions [1]. To address this challenge, in the past many strategies have been proposed in the literature, such as surface chemical modification [3–9], surfactant assistance [10, 11] and other additives incorporation [12, 13].

In terms of preparation techniques, both solvent casting and thermomechanical processing have been extensively used [1, 14, 15]. For solvent-based nanocomposite preparation, the main difficulty is to find a viable solvent to combine CNC, which is hydrophilic, with hydrophobic polymeric matrices. On the other hand, for thermomechanical processing, even in the case where good dispersion is obtained, poor mechanical reinforcement is frequently reported. According to literature [14, 15], this might be a result of CNC shear alignment, which is a consequence of the most common thermomechanical processing techniques. Alignment is an obstacle for CNC percolation phenomena, which has been pointed out as the main mechanism in the CNC reinforcement effect, since the pioneer studies of Favier et al. [14, 16, 17].

In the percolation phenomena, randomly distributed fillers form an interconnected network, which is responsible for the increase in nanocomposite mechanical stiffness [18, 19]. The percolation network is held together by interactions between the dispersed particles (i.e., fillers) [1, 19]. In the CNC case, these interactions are due to hydrogen bonding [17]. To allow the percolation network formation, a minimum CNC content is required as well as random CNC distribution and orientation [1, 17–19]. This minimum content is denominated the percolation threshold (ϕ_c), which is expressed in volume fraction and is usually estimated by the equation proposed by Favier et al. [20]:

$$\phi_c = \frac{0.7}{L/d} \quad (1)$$

where L/d is the nanoparticle aspect ratio.

Poly(ε-caprolactone) (PCL) is a synthetic biopolymer whose flexibility and biodegradability make it a promising candidate for forming nanocomposites with CNC [3, 5]. Aiming to achieve improvement in the polymer properties, PCL/CNC nanocomposites have already been prepared by using various different methods [3, 5, 21–24]. In terms of mechanical properties, nearly all the studies explored the solvent casting methodology, due to the fact that this method exhibits higher reinforcement effect than the thermomechanical processing [14].

Neat CNC nanocomposites, in general, have lower mechanical reinforcement than surface-modified CNC nanocomposites obtained by analogous preparation methods, due to improved particle–matrix adhesion [3, 5, 21]. Consequently, literature reports that Young's modulus improvements greater than 50% were only achieved by using surface-modified CNC [3–5, 21]. As an example, the works of Habibi et al. [5], Hassan et al. [4] and Siqueira et al. [3, 21] showed large PCL reinforcement values, which were around 150%. According to the authors, this behavior is related to the good dispersion of the modified CNC in the PCL matrix [3, 4, 21], as well as to the better particle–matrix interactions [4, 5, 21].

Nevertheless, the CNC surface chemical modification may impair particle–particle interaction, hindering the percolation network formation. Therefore, if percolation is in fact the main mechanism for CNC mechanical reinforcement, as proposed by Favier et al. [17], and it relies on the strong interaction in between adjacent CNC particles, other strategies that favor CNC dispersion, especially in hydrophobic matrices, have to be investigated. One approach, reported by Siqueira et al. [25], is to prepare a physical CNC organogel and then mix it with a polymer solution. Other authors reported the use of water-organic solvent exchange to improve dispersion prior to CNC chemical modification [3, 5, 26]. It is important to point out that, in these works, the solvent exchange methodology is used as a means to improve CNC chemical modification efficiency, while herein this methodology was used as a straightforward approach to improve neat CNC dispersion in the polymer solution.

Therefore, in the present study an alternative methodology to achieve CNC percolation in PCL matrix, avoiding the use of any additives or chemical modification, was investigated. PCL/CNC nanocomposites were prepared by the combination

of solvent exchange and solvent casting methods. Mechanical properties were investigated in order to evaluate the potential to promote mechanical reinforcement. The morphology of the nanocomposites was examined by transmission electron microscopy (TEM) and small angle X-ray scattering (SAXS) techniques. Finally, the correlation between morphology and mechanical properties was addressed in the context of the percolation network formation.

Experimental

Materials

PCL (100 kg mol^{-1}) was purchased from Scientific Polymers (Ontario, USA). A wood pulp-extracted CNC dispersed in aqueous suspension at an 11 wt% concentration was acquired from the University of Maine (Orono, USA) and used without further purification. THF (Synth, São Paulo, Brazil) was used as received.

Solvent exchange

CNC aqueous suspension was submitted to a solvent exchange procedure, using THF as solvent, in order to obtain a CNC organic dispersion. Initially, the aqueous suspension was diluted with deionized water and subsequently with THF, in order to obtain a 4.7 wt% CNC suspension in a solvent mixture containing 60 wt% THF. Afterward, a fractionated THF addition was carried out until 85 wt% THF was achieved. After each dilution, the dispersions were homogenized by vigorous mechanical stirring followed by ultrasonication (81 W, 40 kHz) for 7 min. This process was designed to promote a smooth transition from CNC aqueous suspension to an organic solvent dispersion (Supplementary Material S1).

After the final dilution, the dispersion (1.7 wt% CNC) was homogenized by ultrasonication and then centrifuged for 10 min at 4000 rpm. The resulting precipitate was then washed repeatedly using THF. The supernatant was removed and substituted for pure THF. The dispersion was homogenized and then centrifuged. These steps were repeated three more times to obtain the final CNC organic dispersion.

Solvent casting

PCL was dissolved in THF at room temperature. Afterward, the CNC organic dispersion was added to the PCL solution and left to stir for 24 h. The final dispersion was transferred to Petri dishes and the solvent was removed at room temperature, under constant nitrogen flow. Further details about the precursor dispersion compositions are presented in Table 1. Different PCL/THF mass ratio values were used to prepare precursor mixtures, in order to qualitatively preserve the dispersion viscosity.

Transmission electron microscopy (TEM)

CNC samples were prepared by drying a 5 μL droplet of a 0.01 mg mL^{-1} aqueous suspension over a copper grid coated with ultrathin carbon film. Nanocomposite samples of approximately 50 nm thick were obtained in a cryoultramicrotome Ultracut FC6 (Leica Reichert) using a diamond knife at a − 120 °C temperature. Sample staining with 2 wt% uranyl acetate was used to enhance image contrast. Micrographs were obtained in a JEM 1400 plus microscope (JEOL), operating at a 120-kV acceleration voltage. The images were recorded using a One View camera (Gatan). CNC dimensions were determined from the TEM images (ImageJ software).

Small angle X-ray scattering (SAXS)

SAXS measurements were carried out at the D01B-SAXS1 beamline of the Brazilian Synchrotron Light Laboratory (LNLS-CNPEM) using a monochromatic X-ray beam, $\lambda = 0.1544$ nm, with point collimation. The samples were measured at room temperature

Table 1 Nanocomposite compositions and PCL/THF mass ratios

Material	PCL wt%	CNC wt%	PCL/THF mass ratio
PCL	100	0	0.111
PCL/CNC5	95	5	0.092
PCL/CNC10	90	10	0.087
PCL/CNC15	85	15	0.082
PCL/CNC20	80	20	0.078
PCL/CNC25	75	25	0.073
PCL/CNC30	70	30	0.068
PCL/CNC40	60	40	0.049

using 180 s exposure time. The data were recorded using a Pilatus 300 K hybrid pixel X-ray detector (Dectris) at a 832 mm sample-detector distance. In this configuration, the scattering vector range (q-range) was 0.2 to 5 nm^{-1}, where $q = (4\pi/\lambda)\sin(\theta)$ and 2θ is the scattering angle. Silver behenate was used as standard. In addition to room temperature measurements, temperature-controlled experiments were conducted in a THMS600 hot stage (Linkam). Samples were first kept at 25 °C for 5 min, heated at 10 °C min^{-1} to 90 °C and then maintained at this temperature for 5 min. Measurements were only taken at 25 °C and 90 °C, during the isotherms.

The two-dimensional SAXS data were corrected by the transmitted intensity and the scattering of an empty cell. Azimuthal average was performed with the FIT2D software [27]. Considering that the PCL semicrystalline morphology at the nanoscale is mainly lamellar [28–30], one-dimensional correlation functions were calculated, using the SAXSDAT software [31]. CNC and amorphous PCL (molten state) contributions to the scattering intensity were removed (from the SAXS data) prior to using SAXSDAT software. At the scattering curves, no significant particle–particle interaction was observed at higher CNC contents. All further mathematical operations and data fitting were carried out using Origin(R) software.

Differential scanning calorimetry (DSC)

DSC analyses were performed in a DSC Q2000 (TA Instruments) equipment, using approximately 5 mg samples in flat aluminum pans. The samples were heated from 25 to 100 °C and cooled to − 20 °C with a 5-min isotherm in between. Analyses were carried out under argon atmosphere using a 20 °C min^{-1} heat transfer rate.

To calculate the degree of crystallinity, the following equation was used:

$$\chi = \frac{\Delta H_m}{\Delta H_m^{100\%} \cdot (1 - w_{CNC})} \quad (2)$$

where ΔH_m is the melting enthalpy, $\Delta H_m^{100\%}$ is the enthalpy of 100% crystalline PCL (142 J g^{-1} [32, 33]), and w_{CNC} is the CNC mass fraction.

Dynamical mechanical analysis (DMA)

DMA was carried out in a DMTA V (Rheometric Scientific) equipment in axial tension–compression mode with a 1.0-Hz frequency and a 0.014% amplitude. A − 120 to 40 °C temperature range and a 2 °C min^{-1} heating rate were used. Rectangular sections of 20 × 5 × 0.3 mm were analyzed.

Mechanical properties

Tensile tests were performed based on the ASTM D882-10. At least five test specimens of each sample were submitted to tensile tests in a EMIC 23–20 testing machine (INSTRON) equipped with a 5000 N load cell, using a 10 N preloading and a 150 mm min^{-1} crosshead speed. Test specimens were 10-mm wide and 100-mm-long strips.

Results and discussion

Cellulose nanocrystals

The CNC morphology was characterized by TEM. A micrograph, showing the needle-like shape, which is characteristic of the cellulosic nanoparticles, is presented in Fig. 1. The appearance of bright spherical regions in the micrograph is a direct consequence of staining. Average values for CNC length and

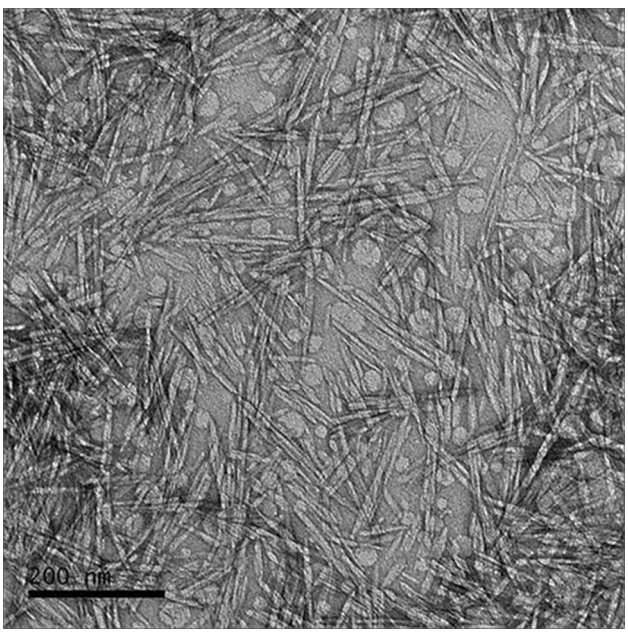

Figure 1 TEM micrograph of CNC.

diameter were found to be 130 ± 50 nm and 7 ± 2 nm, respectively. These values were obtained from 730 measurements, which also provided a 19 ± 8 average aspect ratio. Using this aspect ratio, a 0.037 percolation threshold was calculated by Eq. (1), which corresponds to approximately 5 wt% CNC content in the nanocomposites. The average aspect ratio, determined from TEM images, is similar to some values previously reported in the literature for the nanocrystals from the same supplier [34], although different aspect ratio and/or dimensions values were also reported [13, 35, 36]. These differences can be due to several factors, such as sample preparation and characterization techniques or even to batch variations.

Based on SAXS data from the nanocomposite films in the amorphous state, a 4.0 ± 1.2 nm CNC diameter was determined by fitting a cylindrical form factor to the scattering data (Supplementary Material S2). This value is smaller than the one calculated from TEM (7 ± 2 nm), which can be due to the negative staining used on the TEM characterization. In terms of dimension measurements, the relative error resulting from negative staining is much higher for the diameter than for the length. Hence, the aspect ratio obtained from TEM analysis can be underestimated, which leads to an overestimated percolation threshold (see Eq. 1).

Additional results for the CNC characterization can be found in the Supplementary Material S3 and S4. FTIR analysis was used to confirm the presence of sulfate groups [37] in the CNC surface, which is a result of the sulfuric acid hydrolysis during CNC production [1] (Supplementary Material S3). A 75% crystallinity index value was calculated by the Segal method [38], based on XRD measurements (Supplementary Material S4). Two types of crystalline structures, Cellulose I and Cellulose II, were identified [39].

Nanocomposite thermal and mechanical properties

PCL/CNC nanocomposites, obtained by the combination of solvent exchange and solution casting, were opaque and uniform. (Photographs of the nanocomposite films are shown in Supplementary Material S5.) At the precursor dispersions, shown in Fig. 2, no evidence of CNC sedimentation was observed. This is an indication that the gradual solvent transition from water to THF led to uniform CNC dispersion in the PCL solution, in comparison with dispersions prepared from freeze-dried CNC. It also indicated that the solvent exchange dispersion presented appropriate stability under the solvent casting conditions. To confirm this, the precursor dispersions were observed over time (Fig. 2). The solvent exchange procedure resulted in a kinetically stable dispersion and, consequently, no CNC sedimentation was observed during film casting. In contrast, the dispersions from freeze-dried CNC showed sedimentation after 72 h at rest.

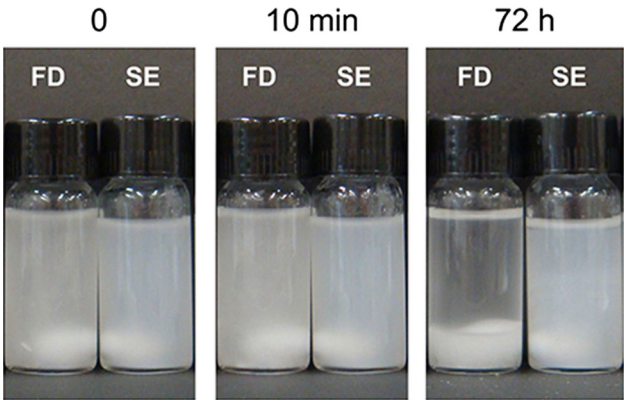

Figure 2 Precursor dispersion stability over time. Dispersions were prepared using freeze-dried CNC (FD) and solvent exchange procedure (SE).

DSC results are summarized in Table 2. (Curves are presented in Supplementary Material S6.) The degree of crystallinity, X, which was 65% on average, showed no significant variations as a function of the CNC content. Moreover, the degrees of crystallinity,

Table 2 Thermal properties for neat PCL and PCL/CNC nanocomposites obtained from DSC analysis

Material	X (%)	T_m °C	$T_{c,onset}$ °C
PCL	65	67	34
PCL/CNC5	65	65	41
PCL/CNC10	65	65	42
PCL/CNC15	66	64	42
PCL/CNC20	62	64	41
PCL/CNC25	66	63	41
PCL/CNC30	65	62	41

X and T_m are the DSC degree of crystallinity and melting temperature, respectively. $T_{c,onset}$ is the cooling onset crystallization temperature

X observed herein are higher than those previously reported in the literature for similar PCL/CNC nanocomposites, however, with smaller PCL molecular weight [3, 5]. In contrast, the PCL crystallization temperature exhibited an increase of approximately 7 °C for the nanocomposites in relation to neat PCL, regardless of the CNC content. This can be due to a CNC nucleating effect on PCL crystallization [23, 24]. The DSC results also showed a progressive reduction of the PCL melting temperature with an increase in the CNC content, changing from 67 °C (neat PCL) to 62 °C (PCL/CNC30 nanocomposite). This behavior can be attributed to a reduction in the average lamellar thickness of the PCL crystalline phase [40].

Figure 3 shows the DMA results for PCL, PCL/CNC5 and PCL/CNC25 nanocomposite films. The normalized loss modulus curves (Fig. 3b) show two transitions: a secondary relaxation at around − 90 °C and an α relaxation, close to − 50 °C, the latter corresponding to PCL glass transition. No variation of the PCL glass transition temperature was observed due to CNC presence. Nevertheless, CNC addition produced broader glass transition peaks, as can be seen in Fig. 3b. This behavior is attributed to materials with a wide range of relaxation times [41], which in this case is due to the presence of CNC that increases the nanocomposite microheterogeneity.

The CNC reinforcement effect on the PCL matrix is visible in the DMA storage modulus results (Fig. 3a) for PCL/CNC nanocomposites, at temperatures above glass transition. However, more conclusive results were extracted from the tensile tests described below. Figure 4 shows Young's modulus and tensile strength as a function of the CNC weight content. Both mechanical properties exhibited an initial reduction with the addition of CNC, when compared to neat PCL. The reduction in tensile strength for PCL/CNC5 nanocomposite is expected, because of the weak interactions between the CNC hydroxyl groups and PCL carbonyl groups and, consequently, to low adhesion at the particle–matrix interface [3, 4, 21]. However, the nanocomposites regain tensile strength with increasing CNC content. This result can be due to the percolation network contribution to the tensile strength, which in turn is due to the increase in particle–particle interaction density. In terms of Young's modulus, the value is also lower for the 5 wt% CNC content in the nanocomposite, compared to neat PCL. Increasing the CNC content, a continuous increase in Young's modulus is observed. The highest mechanical reinforcement was observed for the PCL/CNC25 nanocomposite, which represents a 155% modulus increase in relation to neat PCL.

The CNC percolation network is thought to be formed by a random arrangement of contacting CNC. In their mathematical modeling, Shishehbor et al. [42] discuss the contribution of different interaction forces for a single CNC elastic modulus and show that the longitudinal modulus, which is usually used to represent the CNC modulus, is due to the modulus of individual cellulose chains. Conversely, the interchain hydrogen bonding within the transversal

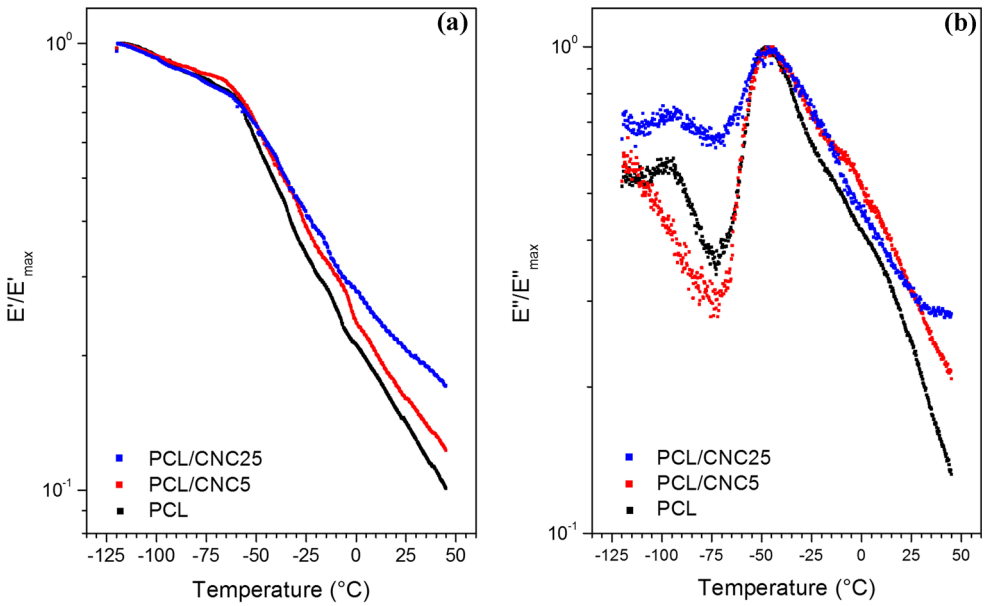

Figure 3 Normalized storage (**a**) and loss (**b**) moduli of neat PCL, PCL/CNC5 and PCL/CNC25 nanocomposites.

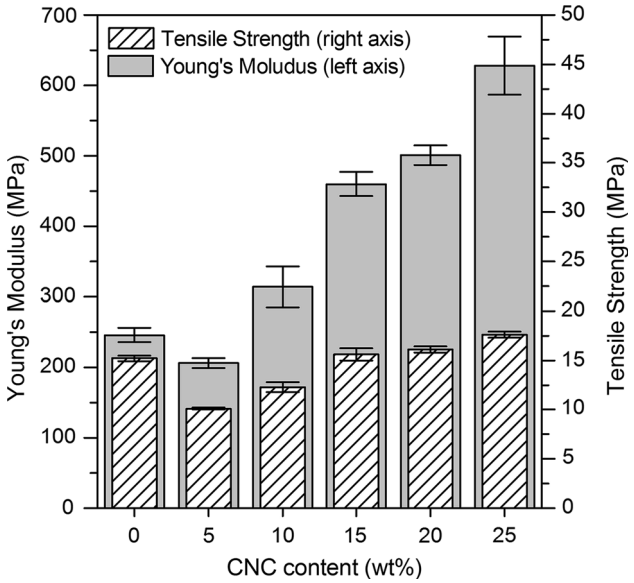

Figure 4 Young's modulus and tensile strength as function of the CNC weight content for the PCL/CNC nanocomposites.

direction has little contribution to the CNC overall modulus. Considering that the hydrogen bonding is the strongest interaction responsible for the CNC contacts [17], it is expected that the percolation network modulus should be lower than the modulus of a single CNC particle. Even though the hydrogen bonding contribution to the overall network modulus is small, it is key to the load transfer in between contacting particles and, therefore, is the main reason for the elevated nanocomposite Young's modulus found herein.

Considering the data reported in the literature, comparable reinforcement was only observed by Habibi et al. [5] and Siqueira et al. [21], however, using surface-modified CNC. Both authors reported reinforcements below 50% when neat CNCs were used for comparison [5, 21]. For neat CNC nanocomposites, the literature only shows lower reinforcements values than the ones found herein. It is also relevant to mention that the majority of these studies concern CNC aspect ratio at least two times higher than the employed in this work.

The above comparison clearly shows the effectiveness of the good nanoparticle dispersion, obtained by this solvent exchange methodology, on the improvement of the PCL/CNC nanocomposite mechanical properties. In spite of the low adhesion between the nanocrystal and the polymer matrix, the use of neat CNC allowed the formation of particle–particle interactions through hydrogen bonding and consequently percolation network formation.

To further evaluate the percolation network formation, the Ouali–Takayanagi equation [16, 43, 44] was used estimate the Young's modulus (E) as a function of the CNC volume fraction (ϕ), as follows:

$$E = \frac{(1-2\upsilon+\upsilon\phi)E_m E_r + (1-\phi)\upsilon E_r^2}{(1-\phi)E_r + (\phi-\upsilon)E_m} \quad (3)$$

where the υ parameter represents the volume fraction of the rigid phase that contributes to the rigidity of the material [44], and E_r and E_m correspond to the modulus of the rigid phase and the matrix, respectively. On the basis of the percolation concept, the dependence of the υ parameter with CNC volume fraction is given by:

$$\upsilon = \begin{cases} 0 & 0 \le \phi \le \phi_c \\ \phi\left(\dfrac{\phi-\phi_c}{1-\phi_c}\right)^b & \phi_c < \phi < 1 \end{cases} \quad (4)$$

where ϕ_c is the percolation threshold and b is the percolation exponent. The percolation exponent value of 0.4 is normally used [17, 19, 20, 44, 45], considering the theoretical results derived by Stauffer and Aharony [46] and De Gennes [47] for three-dimensional percolating systems. In this work, E_m was obtained from the tensile tests shown Fig. 4, while E_r and ϕ_c were used as fitting parameters.

Figure 5 shows Young's modulus data (from Fig. 4) as a function of CNC volumetric fraction, plotted against a percolation model. In this work, the Ouali–Takayanagi, Eq. (3), was used. The overall

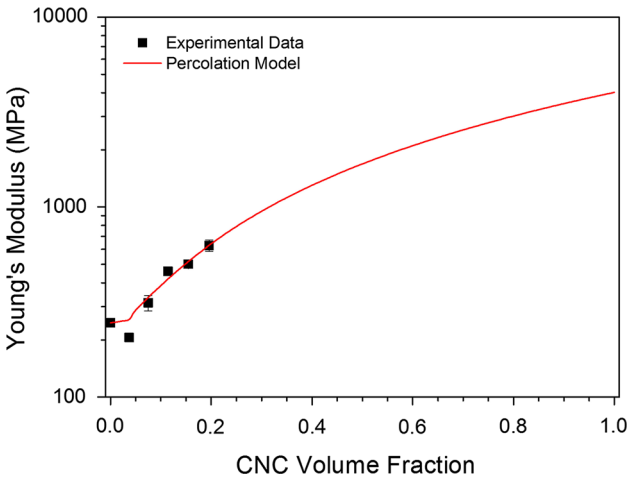

Figure 5 Young's modulus data as a function of the CNC volume fraction (square dots) and Ouali–Takayanagi model fitting (solid line).

fitting of data is good, and provided the E_r and ϕ_c values: 4020 MPa and 0.040, respectively. The E_r value, which represents the modulus of the CNC percolation network, is much lower than the typical values reported for either CNC [42, 48] or cellulose [49]. As discussed above, this is expected since the network is thought to be formed by contacting CNC. The ϕ_c value of 0.04 is in agreement with the 0.037 value calculated from the TEM results and Eq. (1). In addition, the smooth transition in the percolation threshold has also been verified by others and is due to CNC low aspect ratio [45]. Therefore, it is possible to conclude that Eq. (1) is suitable to describe the percolation threshold of PCL/CNC nanocomposites.

Nanocomposite morphology and nanostructure

Figure 6a–c shows low magnification micrographs of neat PCL, PCL/CNC5 and PCL/CNC25 nanocomposites, respectively. In these images, a typical semicrystalline polymer morphology is observed [28]. However, a difference in the contrast patterns can be noticed, when comparing these micrographs, which is related to a mean spherulite size reduction with the CNC content increase. This size reduction is not only due to the nucleation effect, but also to the hindering of lamellar growth caused by the particle barrier effect.

At higher magnification, the PCL/CNC25 nanocomposite presented a clear contrast of the nanoparticles within the polymer matrix (Fig. 6d). The CNC showed good dispersion and random distribution. In addition, it can be noted that the nanoparticles exhibited a certain degree of alignment in localized regions, which is consistent with the CNC distribution between the PCL fibrils. This morphological characteristic had no significant influence on the CNC large-scale orientation, which was random. Therefore, the overall CNC distribution

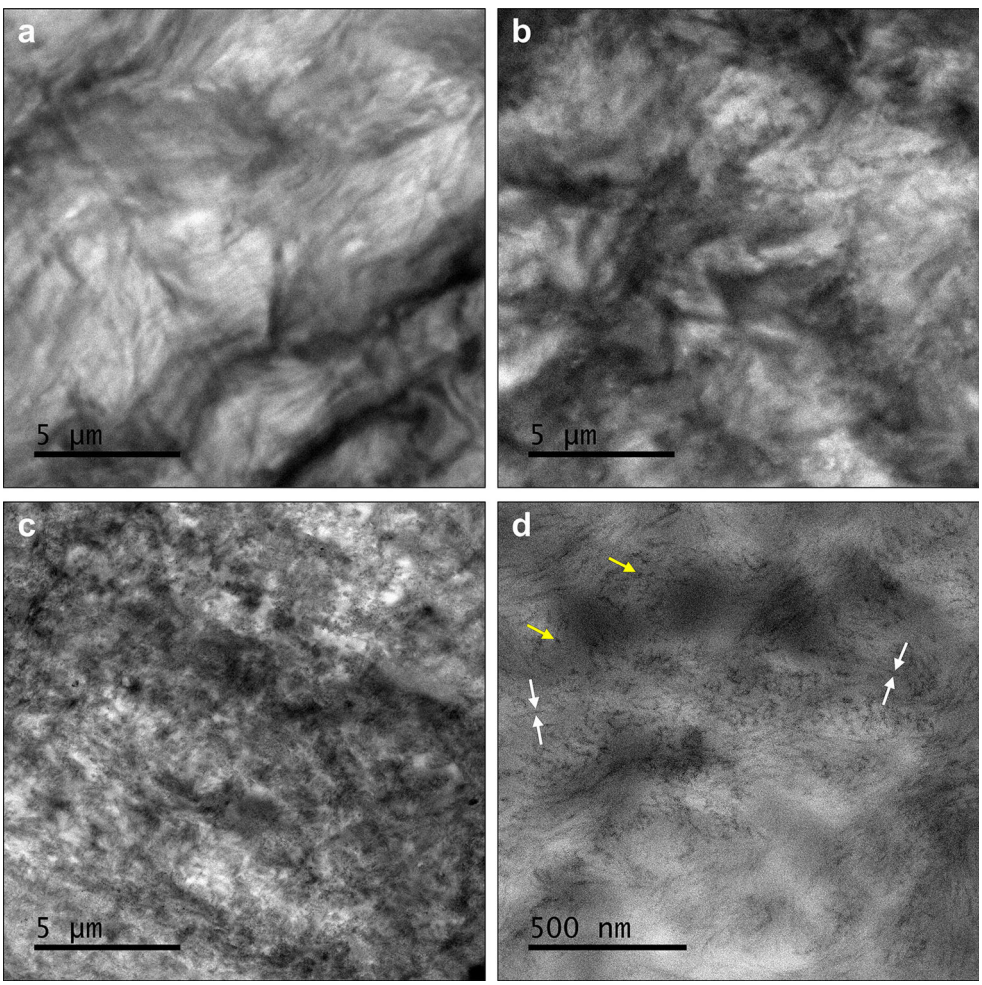

Figure 6 TEM micrographs of neat PCL (**a**), PCL/CNC5 (**b**) and PCL/CNC25 (**c**, **d**) nanocomposites at different magnifications. Yellow and white arrows point to needle-like CNC perpendicular and parallel to the image plane, respectively.

characterized a three-dimensional network within the polymer matrix, i.e., the percolation network. Complementary images at higher magnifications for PCL and nanocomposites are presented in the Supplementary Material S7. The CNC localization in the PCL/CNC5 is not as clear as in the case of PCL/CNC25, due to the staining hindrance caused by the fact that CNCs are isolated within a highly hydrophobic matrix.

The SAXS characterization of the nanocomposites was carried out in order to investigate the CNC distribution in the polymer matrix and its impact in the PCL lamellar parameters. Figure 7 shows the two-dimensional SAXS images of neat PCL and PCL/CNC5 at room temperature as well as the amorphous state (90 °C). The amorphous state is analyzed in order to depict only the features rising from the contrast between crystalline CNC and the amorphous polymeric matrix. Despite a slightly asymmetric pattern for neat PCL (Fig. 7a), all pictures can be considered isotropic, since the scattering intensity showed no significant dependence on the azimuthal angle. Therefore, it was possible to confirm that CNCs are randomly distributed throughout the PCL matrix, in both crystalline (Fig. 7b) and amorphous states (Fig. 7c).

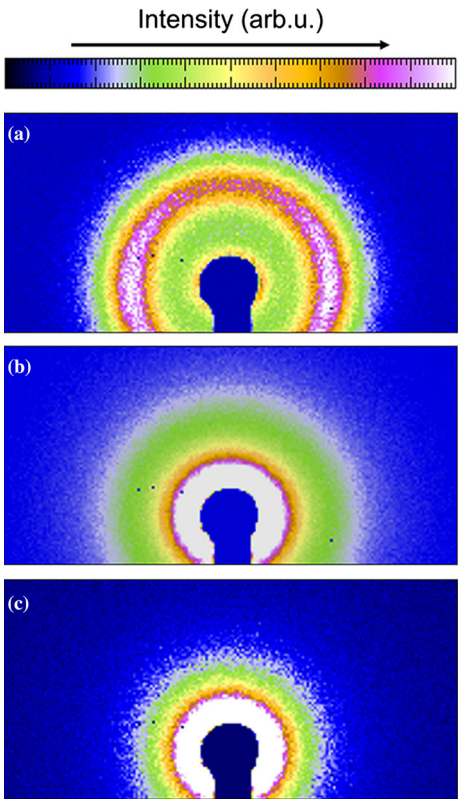

Figure 7 Two-dimensional scattering data for PCL at 25 °C (**a**), PCL/CNC5 nanocomposite at 25 °C (**b**) and PCL/CNC5 nanocomposite at 90 °C (**c**).

Figure 8 shows one-dimensional SAXS curves for neat PCL and PCL/CNC nanocomposites after subtracting the contribution of the CNC nanoparticles to the scattering signal. The original SAXS curves are reported in the Supplementary Material S8.

The PCL SAXS curve shown in Fig. 8 presents a clear main peak at around $q_{max} = 0.42\ nm^{-1}$, which can be attributed to the characteristic periodicity of the lamellar stacks (long period, L) of the PCL semicrystalline morphology. This parameter can be estimated from SAXS curves as $L = 2\pi/q_{max}$ and is approximately 15 nm for the neat PCL. A second-order bump can be noted for higher q; however, it became less apparent at higher CNC content. Another effect of CNC content increase is the progressive shift of the main peak to higher q values. This is a clear indication that CNC promoted morphological alterations in the polymer matrix nanostructure.

In order to obtain further details of the CNC content effect on the PCL matrix, the one-dimensional correlation functions were calculated as defined below [30, 31]:

$$K(r) = \int_0^\infty I(q)q^2 \cos(rq)\mathrm{d}q \tag{5}$$

where r is the distance in Å. The one-dimensional correlation functions are presented in Fig. 9. From

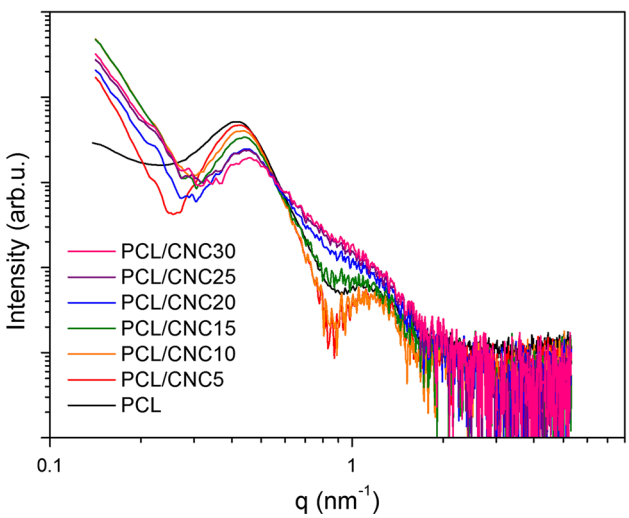

Figure 8 SAXS intensity as a function of the scattering vector for the neat PCL and PCL/CNC nanocomposite films.

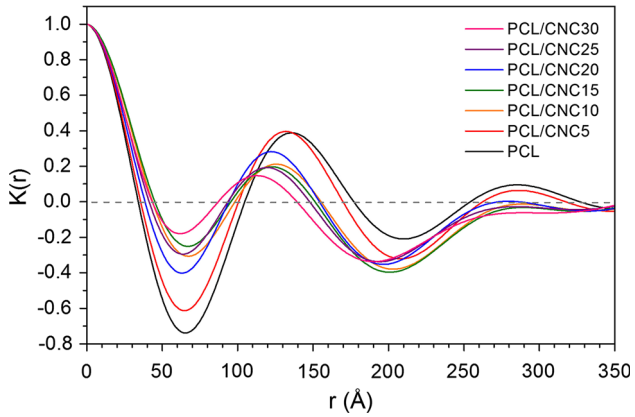

Figure 9 Normalized one-dimensional correlation functions for neat PCL and PCL/CNC nanocomposite films.

these correlation functions, average values for the long period (L), the lamellar thickness (l_c), the interlamellar amorphous thickness (l_a) and the linear degree of crystallinity within the lamellar stacks, which is defined as $X_{lc} = l_c/L$, may be obtained. These parameters are reported in Fig. 10 as a function of the CNC weight content. The parameter's

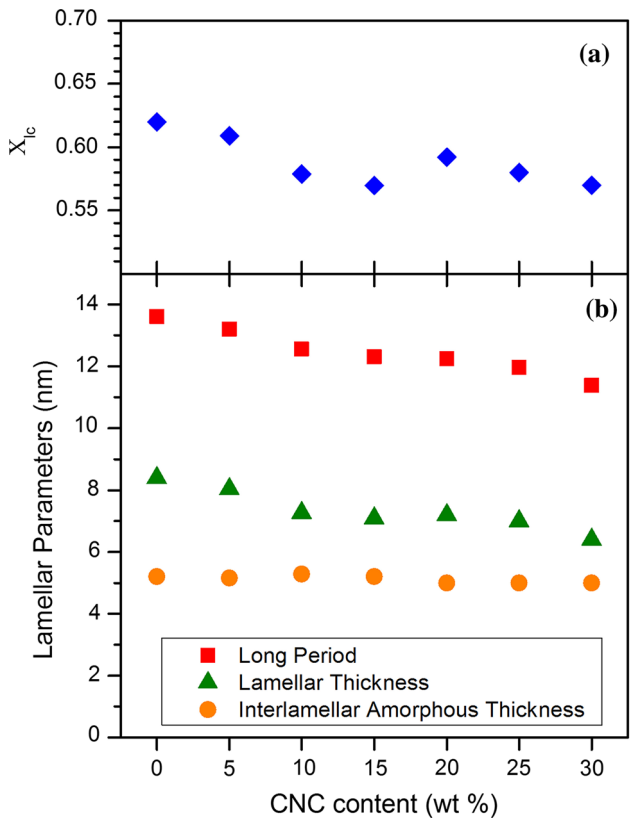

Figure 10 PCL linear degree of crystallinity (**a**) and average lamellar parameters (**b**) as a function of CNC weight content.

estimated errors are smaller than the symbol sizes. Further details on the calculations are provided in the Supplementary Material S8.

The results in Fig. 10b show that the CNC addition promoted a progressive reduction in the long period from 13.6 to 11.3 nm. The PCL lamellar thickness values also decreased with the CNC content, from 8.4 to 6.4 nm. This decrease is in agreement with the DSC results, where a melting temperature reduction was observed as a function of the CNC content. Melting temperature reduction is related to lamellar thickness reduction [40] and is irrespective of the CNC nucleation effect reported earlier (Table 2). The former is dependent on composition, while the latter is not. This is an indication that these results are due to distinct phenomena. Thinner lamellae formation may be caused by polymer chain mobility reduction and confinement, which in turn can be due to CNC presence. The latter is also responsible for hindering the lamellar growth, causing spherulite size reduction (Fig. 6).

Moreover, the interlamellar amorphous region thickness (Fig. 10b) was roughly constant, for all nanocomposite compositions, with a 5.2 nm average value. Comparing the amorphous region thickness with the CNC diameter, it can be concluded that the nanoparticles can hardly be trapped between PCL lamellae during the crystallization process. Therefore, CNC can only be located outside the polymer crystallites, i.e., in between the PCL fibrils and/or the interspherulitic amorphous region.

In relation to the linear degree of crystallinity (Fig. 10a), the obtained values were around 60% and roughly constant with the CNC content. On the other hand, the difference observed between the linear degree of crystallinity (obtained by SAXS) and the degree of crystallinity (obtained by DSC) is small; however, it is expected [28, 50]. Based on this, it can be concluded that the amorphous phase outside the spherulites was scarce, and therefore, it can be considered that the nanocrystals were mainly distributed in the interfibrillar regions. Finally, the variations of PCL lamellar parameters are due to the CNC effect on the polymer crystallization processes during film formation. Although these changes are significant from a morphological point of view, it is not possible to relate them to mechanical reinforcement, which was mainly attributed to the CNC percolation network formation.

Conclusions

The solvent exchange strategy proposed in this work provided a suitable alternative to the CNC chemical modification in the preparation of uniform PCL/CNC nanocomposites and showed expressive mechanical reinforcement. The nanocomposites produced herein exhibited up to a 155% Young's modulus increase. The mechanical behavior of the nanocomposites is in good agreement with the Ouali–Takayanagi percolation model, which showed a 4.02 GPa percolation network modulus.

The combination of TEM and SAXS provided clear insights on the nanocomposite structure and morphology. The nanocomposites presented good CNC dispersion and distribution, allowing the percolation network formation, which was clearly shown in the PCL/CNC25 nanocomposite. SAXS results showed a reduction in the size of the lamellar stack and the lamellae thickness as a function of the CNC content, which is in good correlation with the spherulite size reduction and melting point depression observed in TEM and DSC results, respectively. Based on these findings, it is proposed that the CNCs were preferentially located in the PCL interfibrillar amorphous regions. In conclusion, the solvent exchange methodology developed in this work has proven to be useful for the preparation of mechanically reinforced PCL/neat CNC nanocomposites.

Supplementary material

CNC characterizations: CNC dispersion stability in water-THF mixtures, SAXS characterization results and description, FTIR spectrum and description, and XRD results and description. PCL and nanocomposite characterizations: photographs of the films, DSC curves, SAXS curves and details on data processing, and TEM images.

Acknowledgements

This research was funded by Conselho Nacional de Desenvolvimento Científico e Tecnológico (CNPq, Grant Number 130911/2015-1), Fundação de Amparo à Pesquisa do Estado de São Paulo (FAPESP, Grant Numbers 2010/17804-7, 2016/02414-5) and SPRINT (Grant Number 2017/50274-0). The authors gratefully acknowledge the Brazilian Center for Research in Energy and Materials (CNPEM) laboratories: Center Nanotechnology National Laboratory (LME/LNNano) and staff for the use of TEM facilities, as well as the Brazilian Synchrotron Light Laboratory (LNLS) for the beamtime granted.

Compliance with ethical standards

Conflict of interest The authors declare that they have no conflict of interest.

Electronic supplementary material: The online version of this article (https://doi.org/10.1007/s10853-018-2860-9) contains supplementary material, which is available to authorized users.

References

[1] Dufresne A (2010) Processing of polymer nanocomposites reinforced with polysaccharide nanocrystals. Molecules 15:4111–4128

[2] Azizi Samir MAS, Alloin F, Dufresne A (2005) Review of recent research into cellulose whiskers, their properties and their application in nanocomposite field. Biomacromolecules 6:612–626

[3] Siqueira G, Bras J, Dufresne A (2009) Cellulose whiskers versus microfibrils: influence of the nature of the nanoparticle and its surface functionalization on the thermal and mechanical properties of nanocomposites. Biomacromol 10:425–432

[4] Hassan ML, Bras J, Hassan EA, Fadel SM, Dufresne A (2012) Polycaprolactone/modified bagasse whisker nanocomposites with improved moisture-barrier and biodegradability properties. J Appl Polym Sci 125:E10–E19

[5] Habibi Y, Goffin A-L, Schiltz N, Duquesne E, Dubois P, Dufresne A (2008) Bionanocomposites based on poly(ε-caprolactone)-grafted cellulose nanocrystals by ring-opening polymerization. J Mater Chem 18:5002–5010

[6] Araki J, Wada M, Kuga S (2001) Steric stabilization of a cellulose microcrystal suspension by poly(ethylene glycol) grafting. Langmuir 17:21–27

[7] de Oliveira Taipina M, Ferrarezi MMF, Yoshida IVP, Gonçalves MDC (2013) Surface modification of cotton nanocrystals with a silane agent. Cellulose 20:217–226

[8] Qian S, Sheng K, Yu K, Xu L, Fontanillo Lopez CA (2018) Improved properties of PLA biocomposites toughened with bamboo cellulose nanowhiskers through silane modification.

J Mater Sci 53:10920–10932. https://doi.org/10.1007/s10853-018-2377-2

[9] Junior de Menezes A, Siqueira G, Curvelo AAS, Dufresne A (2009) Extrusion and characterization of functionalized cellulose whiskers reinforced polyethylene nanocomposites. Polymer 50:4552–4563

[10] Ljungberg N, Cavaillé JY, Heux L (2006) Nanocomposites of isotactic polypropylene reinforced with rod-like cellulose whiskers. Polymer 47:6285–6292

[11] Mariano M, Pilate F, De Oliveira FB, Khelifa F, Dubois P, Raquez JM, Dufresne A (2017) Preparation of cellulose nanocrystal-reinforced poly(lactic acid) nanocomposites through noncovalent modification with PLLA-based surfactants. ACS Omega 2:2678–2688

[12] Meesorn W, Shirole A, Vanhecke D, De Espinosa LM, Weder C (2017) A simple and versatile strategy to improve the mechanical properties of polymer nanocomposites with cellulose nanocrystals. Macromolecules 50:2364–2374

[13] Nagalakshmaiah M, Pignon F, El Kissi N, Dufresne A (2016) Surface adsorption of triblock copolymer (PEO–PPO–PEO) on cellulose nanocrystals and their melt extrusion with polyethylene. RSC Adv 6:66224–66232

[14] Dufresne A (2008) Polysaccharide nanocrystal reinforced nanocomposites. Can J Chem 86:484–494

[15] Oksman K, Aitomäki Y, Mathew AP, Siqueira G, Zhou Q, Butylina S, Tanpichai S, Zhou X, Hooshmand S (2016) Review of the recent developments in cellulose nanocomposite processing. Compos Part A Appl Sci Manuf 83:2–18

[16] Favier V, Canova GR, Cavaillé JY, Chanzy H, Dufresne A, Gauthier C (1995) Nanocomposite materials from latex and cellulose whiskers. Polym Adv Technol 6:351–355

[17] Favier V, Canova GR, Shrivastava SC, Cavaille JY (1997) Mechanical percolation in cellulose whisker nanocomposites. Polym Eng Sci 37:1732–1739

[18] Fralick BS, Gatzke EP, Baxter SC (2012) Three-dimensional evolution of mechanical percolation in nanocomposites with random microstructures. Prob Eng. Mech. 30:1–8

[19] Loos MR, Manas-Zloczower I (2013) Micromechanical models for carbon nanotube and cellulose nanowhisker reinforced composites. Polym Eng Sci 53:882–887

[20] Favier V, Dendievel R, Canova G, Cavaille JY, Gilormini P (1997) Simulation and modeling of three-dimensional percolating structures: case of a latex matrix reinforced by a network of cellulose fibers. Acta Mater 45:1557–1565

[21] Siqueira G, Bras J, Follain N, Belbekhouche S, Marais S, Dufresne A (2013) Thermal and mechanical properties of bio-nanocomposites reinforced by Luffa cylindrica cellulose nanocrystals. Carbohydr Polym 91:711–717

[22] Wang W, Liu D, Lu L, Chen H, Gong T, Lv J, Zhou S (2016) The improvement of the shape memory function of poly(ε-caprolactone)/nano-crystalline cellulose nanocomposites via recrystallization under a high-pressure environment. J Mater Chem A 4:5984–5992

[23] Lv Q, Xu C, Wu D, Wang Z, Lan R, Wu L (2017) The role of nanocrystalline cellulose during crystallization of poly(ε-caprolactone) composites: nucleation agent or not? Compos Part A Appl Sci Manuf 92:17–26

[24] Siqueira G, Fraschini C, Bras J, Dufresne A, Prud'homme R, Laborie M-P (2011) Impact of the nature and shape of cellulosic nanoparticles on the isothermal crystallization kinetics of poly(ε-caprolactone). Eur Polym J 47:2216–2227

[25] Siqueira G, Mathew AP, Oksman K (2011) Processing of cellulose nanowhiskers/cellulose acetate butyrate nanocomposites using sol–gel process to facilitate dispersion. Compos Sci Technol 71:1886–1892

[26] Xu C, Chen J, Wu D, Chen Y, Lv Q, Wang M (2016) Polylactide/acetylated nanocrystalline cellulose composites prepared by a continuous route: a phase interface-property relation study. Carbohydr Polym 146:58–66

[27] Hammersley AP, Svensson SO, Thompson A, Graafsma H, Kvick E, Moy JP (1995) Calibration and correction of distortions in two-dimensional detector systems[a]. Rev Sci Instrument 66:2729–2733

[28] Plivelic S, Cassu SN, do Carmo Gonçalves M, Torriani IL (2007) Structure and morphology of poly(ε-caprolactone)/chlorinated polyethylene (PCL/PECl) blends investigated by DSC, simultaneous SAXS/WAXD, and elemental mapping by ESI-TEM. Macromolecules 40:253–264

[29] Wurm A, Lellinger D, Minakov AA, Skipa T, Pötschke P, Nicula R, Alig I, Schick C (2014) Crystallization of poly(ε-caprolactone)/MWCNT composites: a combined SAXS/WAXS, electrical and thermal conductivity study. Polymer 55:2220–2232

[30] Strobl GR, Schneider M (1980) Direct evaluation of the electron density correlation function of partially crystalline polymers. J Polym Sci Polym Phys Ed 18:1343–1359

[31] Rabiej S, Rabiej M (2011) Determination of the parameters of lamellar structure of semicrystalline polymers using a computer program SAXSDAT. Polimery 56:662–670

[32] Tsuji H, Ikada Y (1998) Blends of aliphatic polyesters. II. Hydrolysis of solution-cast blends from poly(L-lactide) and poly (ε-caprolactone) in phosphate-buffered solution. J Appl Polym Sci 67:405–415

[33] Crescenzi V, Manzini G, Calzolari G, Borri C (1972) Thermodynamics of fusion of poly-β-propiolactone and poly-ε-caprolactone. Comparative analysis of the melting of aliphatic polylactone and polyester chains. Eur Polym J 8:449–463

[34] Girouard N, Schueneman GT, Shofner ML, Meredith JC (2015) Exploiting colloidal interfaces to increase dispersion,

performance, and pot-life in cellulose nanocrystal/waterborne epoxy composites. Polymer 68:111–121
[35] Mariano M, El Kissi N, Dufresne A (2015) Melt processing of cellulose nanocrystal reinforced polycarbonate from a masterbatch process. Eur Polym J 69:208–223
[36] Hoeng F, Denneulin A, Neuman C, Bras J (2015) Charge density modification of carboxylated cellulose nanocrystals for stable silver nanoparticles suspension preparation. J. Nanoparticle Res 17:244
[37] Socrates G (2001) Infrared and Raman characteristic group frequencies, 3rd edn. Wiley, New York
[38] Segal L, Creely JJ, Martin AE Jr, Conrad CM (1959) An empirical method for estimating the degree of crystallinity of native cellulose using the X-ray diffractometer. Text Res J 29:786–794
[39] Klemm D, Heublein B, Fink HP, Bohn A (2005) Cellulose: fascinating biopolymer and sustainable raw material. Angew Chemie Int Ed 44:3358–3393
[40] Bower DI (2002) An introduction to polymer physics, 1st edn. Cambridge University Press, Cambridge
[41] Koleske JV, Lundberg RD (1969) Lactone polymers. I. Glass transition temperature of poly-ε-caprolactone by means of compatible polymer mixtures. J Polym Sci Part A 7:795–807
[42] Shishehbor M, Dri FL, Moon RJ, Zavattieri PD (2018) A continuum-based structural modeling approach for cellulose nanocrystals (CNCs). J Mech Phys Solids 111:308–332
[43] Takayanagi M, Uemura S, Minami S (1964) Application of equivalent model method to dynamic rheo-optical properties of crystalline polymer. J Polym Sci Part C Polym Symp 5:113–122
[44] Ouali N, Cavaille JY, Perez J (1991) Elastic, viscoelastic and plastic behavior of multiphase polymer blends. Plast Rubber Compos Process Appl 16:55–60
[45] Sapkota J, Martinez Garcia JC, Lattuada M (2017) Reinterpretation of the mechanical reinforcement of polymer nanocomposites reinforced with cellulose nanorods. J Appl Polym Sci 134:45354
[46] Stauffer D, Aharony A (1994) Introduction to Percolation theory, 2nd edn. Taylor & Francis, London
[47] De Gennes PG (1979) Scaling concepts in polymer physics, 1st edn. Cornell University Press, Ithaca
[48] Lahiji RR, Xu X, Reifenberger R, Raman A, Rudie A, Moon RJ (2010) Atomic force microscopy characterization of cellulose nanocrystals. Langmuir 26:4480–4488
[49] Tashiro K, Kobayashi M (1991) Theoretical evaluation of three-dimensional elastic constants of native and regenerated celluloses: role of hydrogen bonds. Polymer 32:1516–1526
[50] Debier D, Jonas AM, Legras R (1998) Blends of polycarbonate and acrylic polymers: crystallization of polycarbonate. J Polym Sci Part B Polym Phys 36:2197–2210